On the Structure and Variability of the Filchner Overflow Plume.

Arne Foldvik, Tor Gammelsrød, Terje Restad and Svein Østerhus.
Geophysical Institute, University of Bergen, 5008 Bergen, Norway

1. Introduction

The southern Weddell Sea is covered by the floating Filchner – Ronne Ice Shelf. Outside the ice shelf, where a polynya is kept open by tides and winds, conditions are often favourable for ice formation. High Salinity Shelf Water (HSSW, T~ -1.9°C, S>34.65) is formed here by freezing and brine rejection. Some of the HSSW flows underneath the floating ice shelf (Foldvik et al 2001). Here it is cooled further in contact with the meteoric ice at great depths where the freezing point is below –1.9°C, and thus Ice Shelf Water (T<-1.9°C) is formed. Drilling through near 800m thick ice south of Berkner Island (Nicholls et al 2001) has shed new light on the processes below the ice shelf. Their measurements seem to confirm a hypothesis forwarded by Foldvik and Gammelsrød (1988) that the HSSW formed on the shallow Berkner shelf flows around the Berkner Island to exit on the west flank on the Filchner Depression, see map in Fig.1. Most of the ISW overflows the Filchner sill at about 74°40'S. Passing the sill its density is higher than the water mass residing her, so it forms a bottom trapped plume.

In this paper we look at some aspects of the basic dynamics of this plume. We present near synoptic bottom temperatures and CTD sections across the plume. The time variability is discussed using current measurements. Based on these we discuss the basic physics of the plume. Topographic steering, thermobaric effects and supercritical flow appear to be key elements in describing the plume.

Bottom water formation in the Antarctic is a key issue in global thermohaline circulation and therefore global climate. It is believed that more than half of the Antarctic bottom water is formed in the Weddell Sea (Orsi et al 1999). The Filchner overflow plumes discussed here also contribute to this bottom water formation, Foldvik and Gammelsrød (1988), and may in fact be one of the dominant sources.

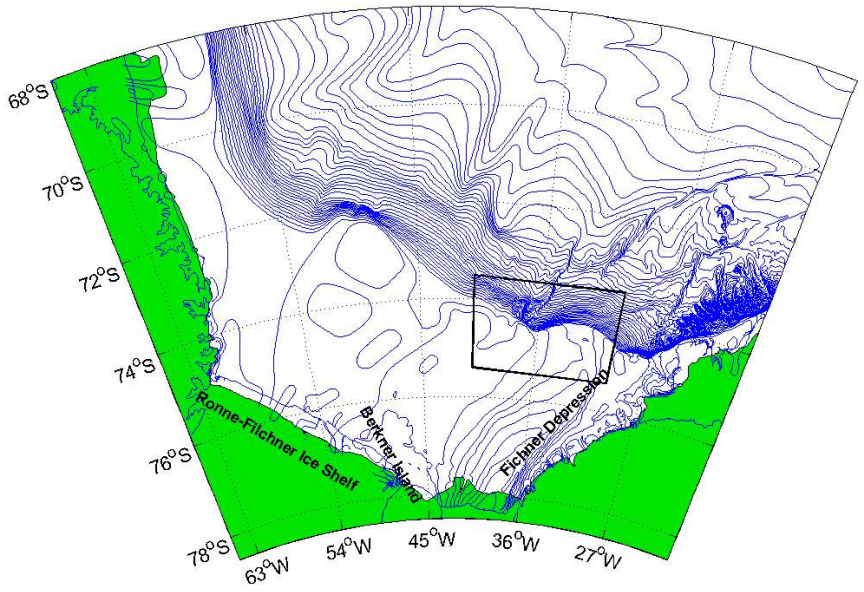

Fig.1. Bottom topography (GEBCO) of the Weddell Sea. Study area indicated.

2. Bottom Temperature

The bottom temperatures based on the 1985 CTD survey with KV "Andenes" on the shelf and slope, are shown in Fig.2. ISW plumes have been observed in this area a number of times since they first were detected in 1977 (Foldvik et al, 1985, see Nicholls et al, 2001 for a recent example). The ISW leaves the sill at about 700 meters depth, turn west as it passes the shelf break and then continues down-slope. From Fig.2 an angle between the plume direction and the isobaths is observed to be roughly 20°. At about 36°W the current appears to be steered by a ridge towards the northeast. ISW was here observed deeper than the 2000-meter level.

The lines marked with capital letters A-D in Fig.2 denote CTD-sections across the plume. These sections are shown in Fig.3. The cold bottom trapped plume is about 10 km wide and has a maximum thickness of around 100 meters. The fact that the plume was warmer at section B and C than at A and D, is not a result of space variability, but rather non-stationarity. The sections were taken in order C, B, A, during a few days, whereas section D was taken about two weeks later. Thus the cold water observed at section A may have penetrated all the way down to section D during this period. Furthermore, the slightly warmer plumes at section B and C are also more saline than the plumes at sections A and D, possibly indicating that the warmer plume is derived from HSSW, see Schlosser et al. (1990).

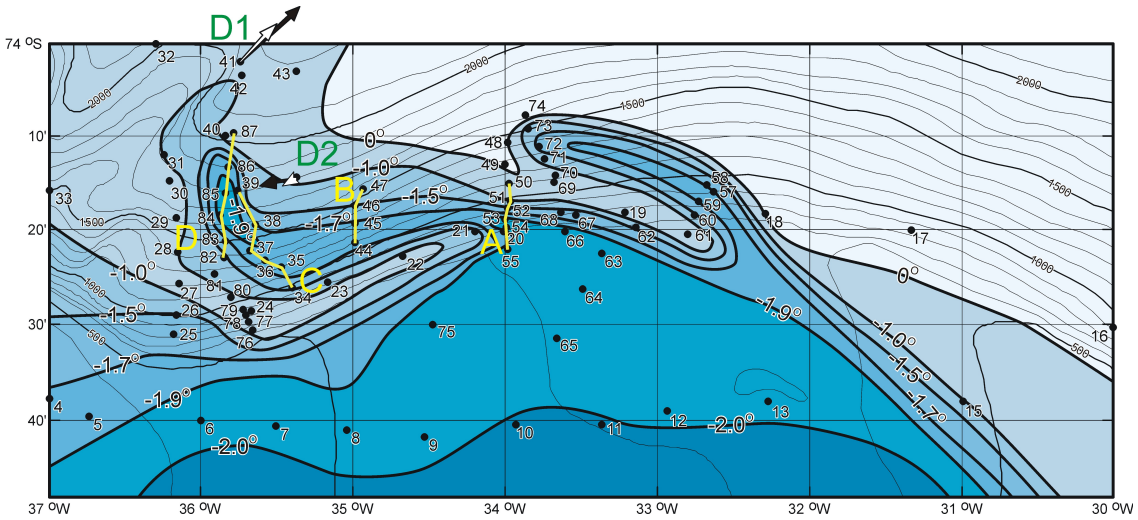

Fig. 2. Bottom temperatures obtained from a CTD survey in 1985. Dots indicate CTD stations and the adjacent numbers the station numbers. Lines marked A-D show positions of the CTD sections shown in Fig.3. Average currents from positions D1 and D2 are also shown.

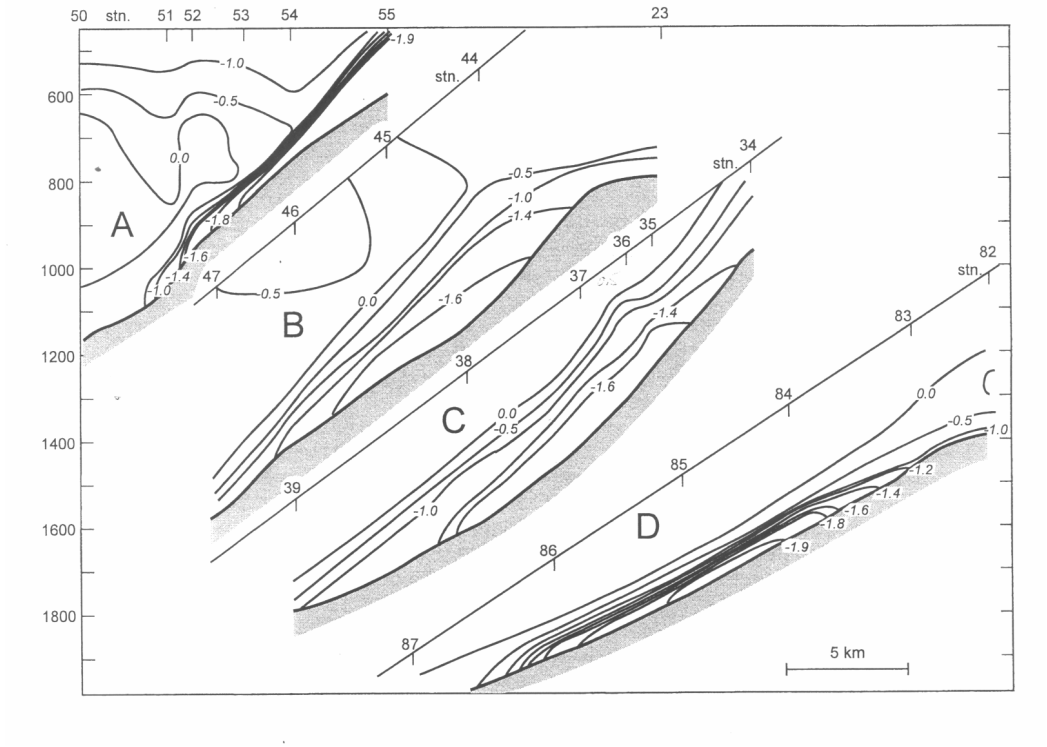

Fig.3. CTD sections on the slope obtained in 1985, see Fig2 for positions.

More details of the plume structure may be observed in a densely spaced section obtained with K/V Andenes in 1990, see Fig.4. This section was located near 34°10'W, slightly west of section A (not shown in Fig.2). Here it seems like two different cold (T<-1.9°C) plumes are interacting. One ISW plume centred near 1200m depth is associated with a local maximum in salinity (>34.6). Another bottom plume, indicated by the thick –1.9°C water layer centred near station B52 at about 1000m depth, seems to be over-riding the more saline plume further down on the slope. Temperature and salinity profiles from station B54 (Fig.5), illustrate that a ~30m thick ISW bottom layer is intersected by a thin, slightly more saline and warmer layer around 1060m depth, while another cold plume of ISW was observed above between 1000 and 1040m depth.

3. Current measurements.

The average currents are strongly guided by the bottom topography. However, currents occasionally show high variability on a time scale of about 30 hours, see Fig.6. The first 2 months of speed measurements at position D2 at the level 25 meters above bottom (mab) is shown in Fig.6a. The position is indicated in Fig.2. The currents are often very strong, i.e. above 0.5 ms^{-1}. Occasionally a quasi-periodic phenomenon with period longer than the diurnal tides shows up. This wavy structure is particularly clear the last 10 days of March, and the current vector for that period is shown in Fig.6b (tides filtered out). The average current direction is westwards parallel to the isobaths. The cross-isobath speed (u) and temperature are shown in Fig.6c, and the along-isobath speed and temperature for the same 10-day period are shown in Fig.6d. In Figs. 6c and 6d tides are still included. We note that high down-slope (u>0) speeds, as well as high westward (v<0) speeds are correlated with low temperatures.

The current vectors at position D1 (for position see Fig.2) for the last 10 days in March is shown in Fig.7. Here the current is much more uni-directional than at D2. An inspection of the topography in Fig.2 indicates that the current is steered in the direction NNE by a steep underwater ridge. The current is stronger at D1 than at D2. This is demonstrated in Fig.8, where we have shown the temperature - speed scatter plots from D1 and D2 at 25m and 100 m above bottom. The strong correlation between the speed and temperature is clearly seen except at position D2, 100mab. The high temperatures at D2 indicate that the ISW plume seldom was as thick as 100m here.

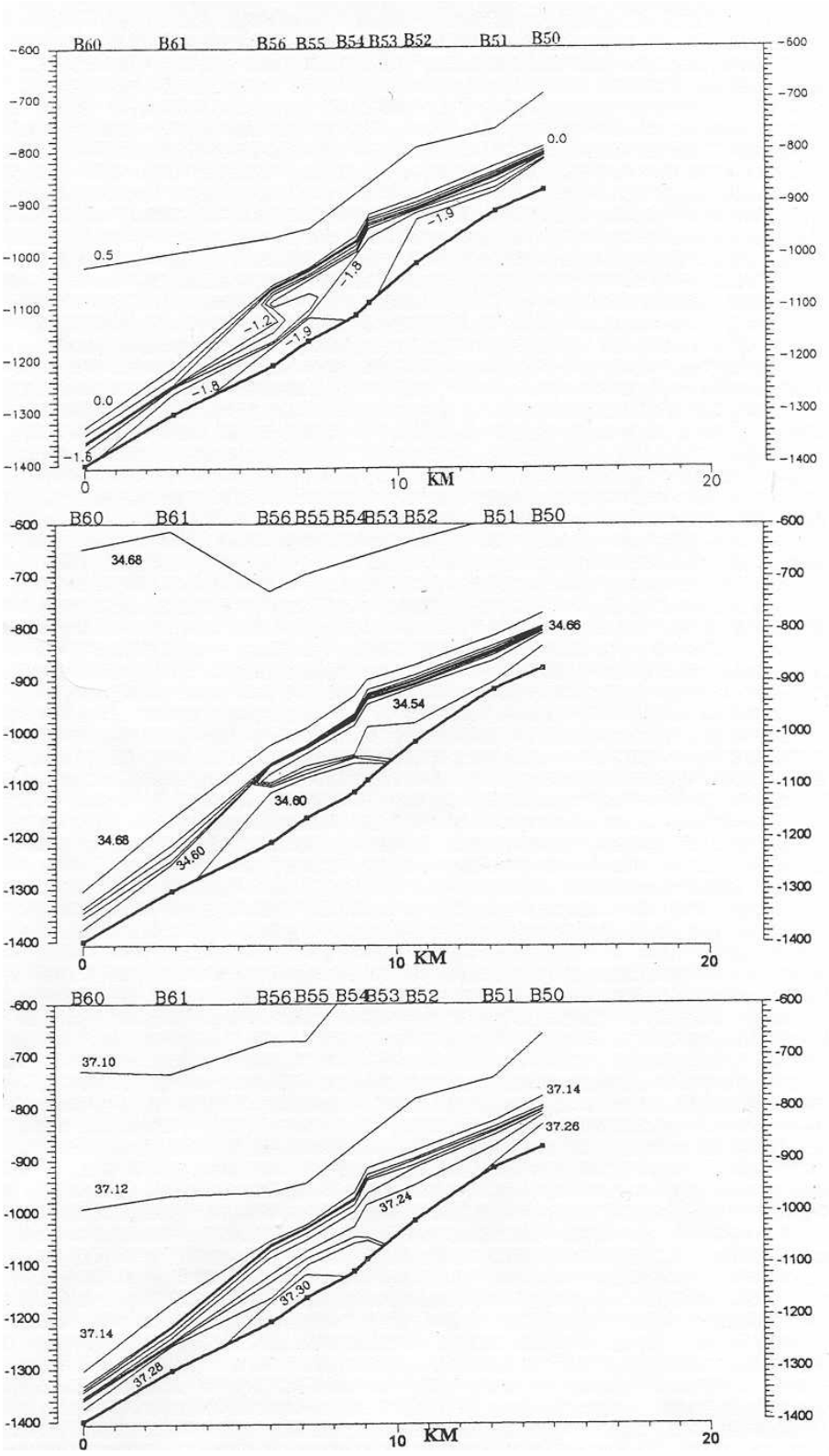

Fig.4. A CTD section obtained in 1990, located near 34° 10'W, i.e. a little west of section A in Fig.2. a)Temperature, b) Salinity and c) Density calculated relative to 2000db.

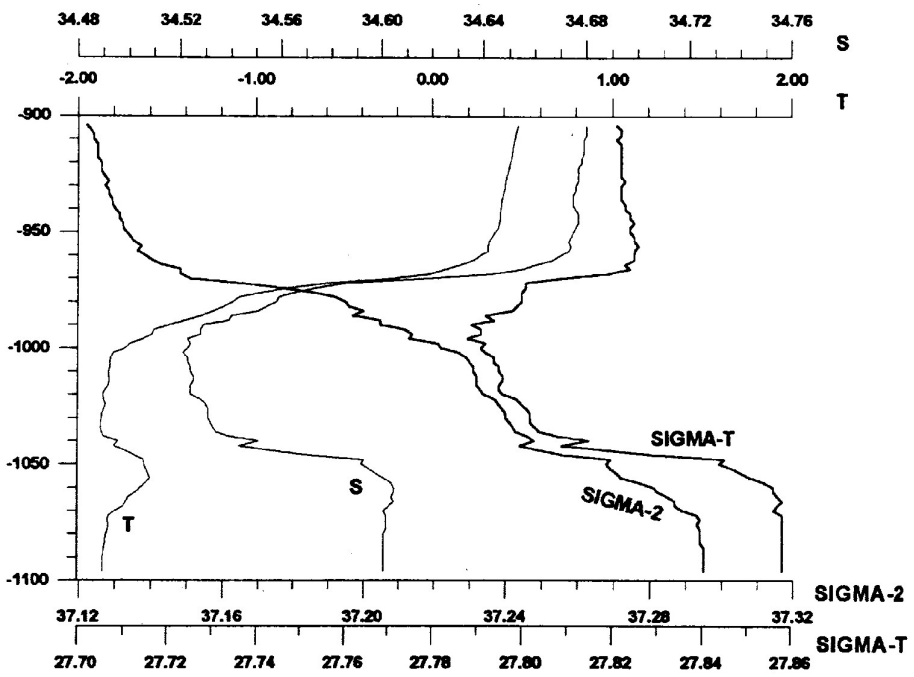

Fig.5. Temperature, salinity and density profiles of the lower 220m layer at station B54 shown in Fig.4. Density profiles computed with both 2000db and 0db as reference levels are shown.

4. Discussion

Topographic steering.

According to the principle of conservation of potential vorticity, the quantity

$$(1) \qquad \frac{d}{dt}\left(\frac{f+\zeta}{D}\right) = 0$$

where f is the Coriolis parameter, ς is the relative vorticity and D is the thickness of the plume. It is common to disregard the relative vorticity ς compared to the planetary vorticity f, and since we are studying a limited area, f may also be assumed constant. Equation 1) then expresses that D is conserved along stream-lines. For horizontal flows the current then must follow the isobaths. When the isobaths converge down-stream the speed must increase because of continuity. Otherwise the thickness of the plume has to increase, violating our assumption. Let L denote the horizontal distance between two isobaths. The isobaths converge and the distance between them is reduced to L-ΔL. Flow continuity require

$$(2) \qquad L\ \Delta v_0 = [L - \Delta L]\ \Delta v$$

where Δv_0 and Δv denote the velocity difference across the plume interface before and after the convergence of the isobaths.

Assuming that the flow is geostrophic the velocity difference between the plume and the water above is given by the tilt of the interface:

(3) $\Delta v_0 = (g'/f)\, h/L,$

where g' is the reduced gravity $g' = g\, \Delta\rho/\rho$, f is the Coriolis parameter and h/L is the tilt of the interface. From equations (2) and (3) follows

(4) $\Delta v = L/(L-\Delta L)\, \Delta v_0 = (g'/f)h/(L-\Delta L)$

Thus, the tilt of the interface responds to changes in the bottom slope. In particular, if the interface is parallel to the bottom at the outset it will remain parallel to the bottom.

The tilt of the interface may be taken from Fig.4 c, and shows that it varies between 0.02 and 0.05. Using $f = 1.3*10^{-4}$ s^{-1}, $g' = 10^{-3}$ ms^{-2} from Fig.4c, we obtain from equation (3) that the velocity jump across the interface is between 0.2 and 0.6 ms^{-1}. This may be compared with the current speed inside and outside the plume in position D2. A measure for the velocity difference between the plume and the water above may be obtained by calculating the average speed at D2 100 mab (0.14ms^{-1}) and the average speed when the water temperature is <-1.0°C at 25 mab (0.45ms^{-1}). The result is 0.3 ms^{-1}, i.e. within the range of the theoretical values.

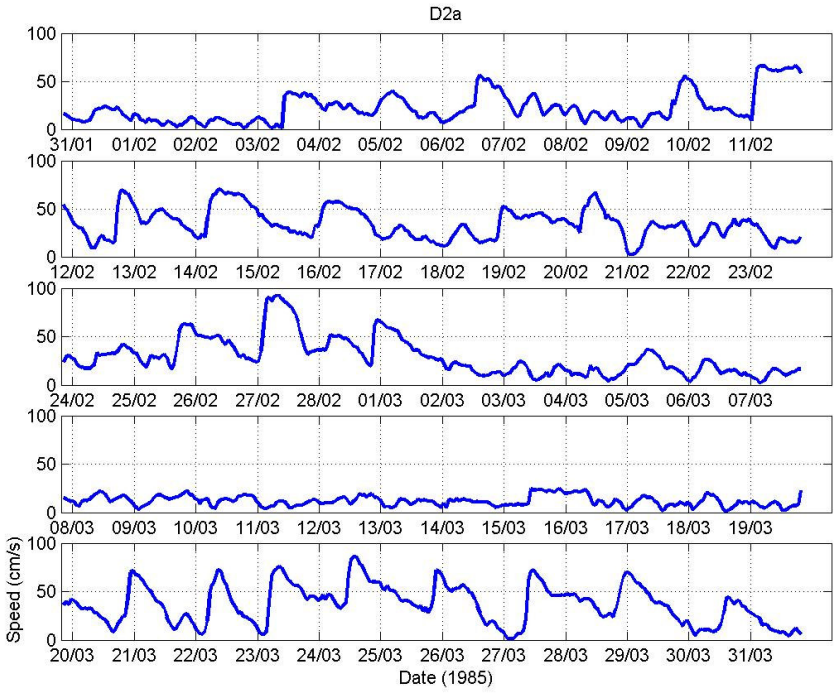

Fig.6a. First 2 months of recorded speed at position D2, 25 m.a.b. The sampling interval was 1 hour. The data is unfiltered. Bottom depth is 1800m. See Fig.2 for position and average current.

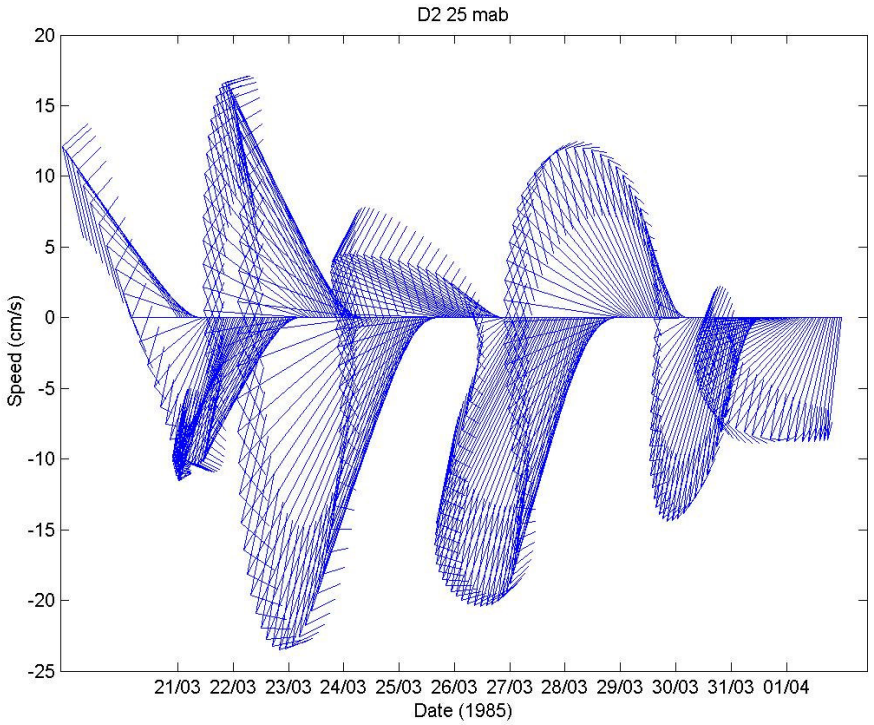

Fig.6b Current vectors of the last 12 days in March for D2, 25mab. Tides filtered out. North is up.

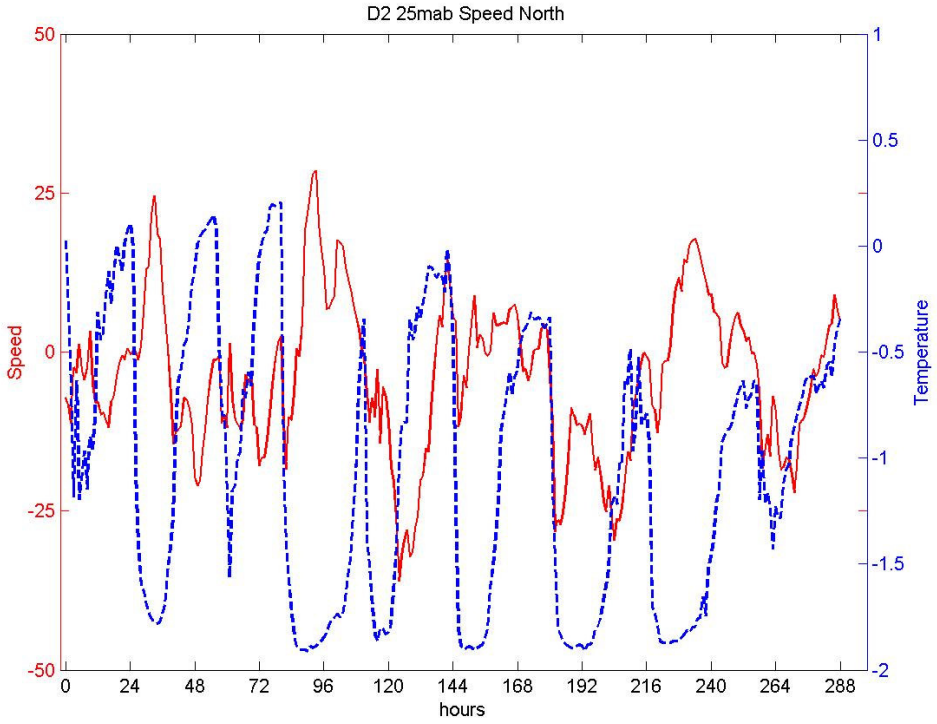

Fig.6c. Meridional speed (up/down- slope)(——) and temperature(- - - -) last 12 days in March for D2, 25mab

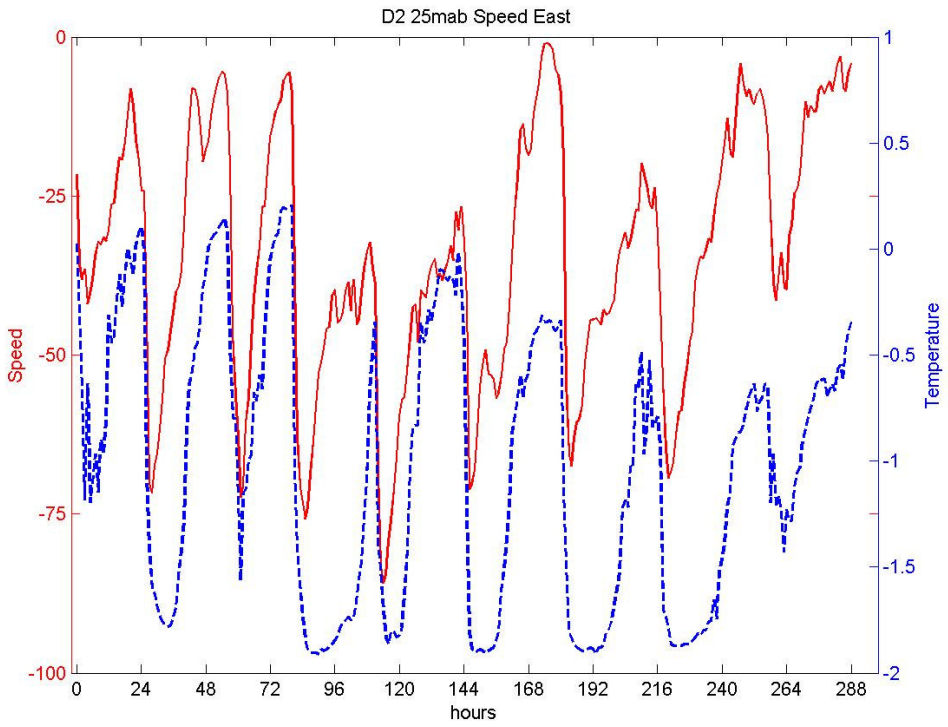

Fig.6d . *Zonal speed, i.e. along-slope (positive east)(——) and temperature (- - - -) the last 12 days in March for D2, 25mab*

If we compare the current speeds at D1 and D2 (Figs 7 and 8) we find that the average speed at D1 (37 cm s^{-1}) is near twice as high as D2 (20 cm s^{-1}). By inspecting the bottom topography (see map in Fig.2) we find that the continental slope is steeper at D1 than at D2 (0.040 compared to 0.025). Thus the ratio between the slopes (D1/D2) is 1.60, while the ratio between the average speeds is 1.85. This indicates that topographic steering is important for the plume dynamics.

Plume dynamics with friction

According to the theory discussed above the cold plumes are assumed aligned along the isobaths, and would never be able to penetrate to large depths, as observed here. Friction is of course a candidate for the transport of cold plume water down the slope. The Ekman transport in the benthic boundary layer has a downward component, which certainly is contributing all the time.

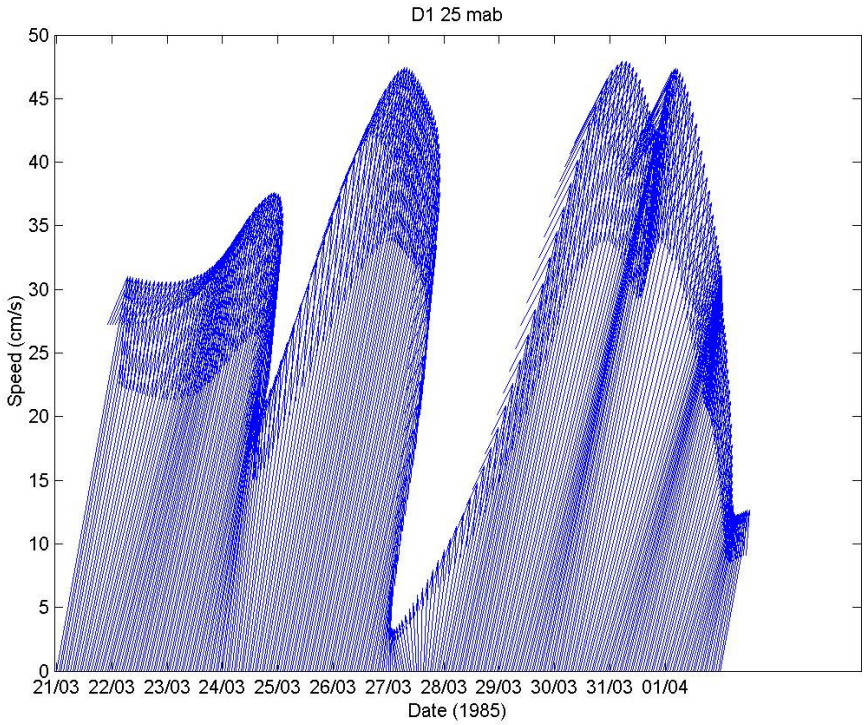

Fig.7 Current vectors of the last 12 days in March for D1, 25mab. Tides filtered out. North is up.

If we think of the plume as a slab current, friction against the bottom and friction and entrainment from the layer above will steer the current at an angle down-slope. This angle β, may be calculated if we assume the following momentum balance at a bottom with slope h/L = $tan\alpha \approx \alpha$;

Cross plume balance;

(5) $0 = g'\sin\alpha\cos\beta - fv$ (cross stream buoyancy – Coriolis)

and along plume balance;

(6) $0 = g'\sin\alpha\sin\beta - \frac{v^2}{D}(C_d^{\ eff})$ (along stream buoyancy – friction)

Here v is the plume speed and D is the thickness of the plume. C_d^{eff} includes both skin friction and entrainment and depends critically on the Richardson number (Alendal et al. 1994).

From Fig.2 the bottom slope in the vicinity of D2 is about α~2° and the isotherms intersect the isobaths with and angle β~20°. Solving equations 5 and 6 with respect to β, using D = 100m, and the maximum for $C_d^{eff} = 1.8\ 10^{-2}$ valid for Ri=1 (Alendal et al 1994), we obtain β = 17°.

Fig.6 indicates the importance of the various terms in the equations of motion. First of all the variability is very large, so the assumption of stationarity is not valid. The bottom topography is here oriented near E-W, so the pure geostrophic current will be oriented towards W, which compares well with the average current. Fig6c indicates that low temperature is related to strong down-slope component of the current. When the speed increases, so does the Coriolis force, which will turn the currents back uphill. Then both buoyancy and friction will slow down the current, and the buoyancy will turn it back downhill. Thus the periodic behaviour of the plume at this location may be explained by the interplay between the buoyancy, friction and Coriolis forces.

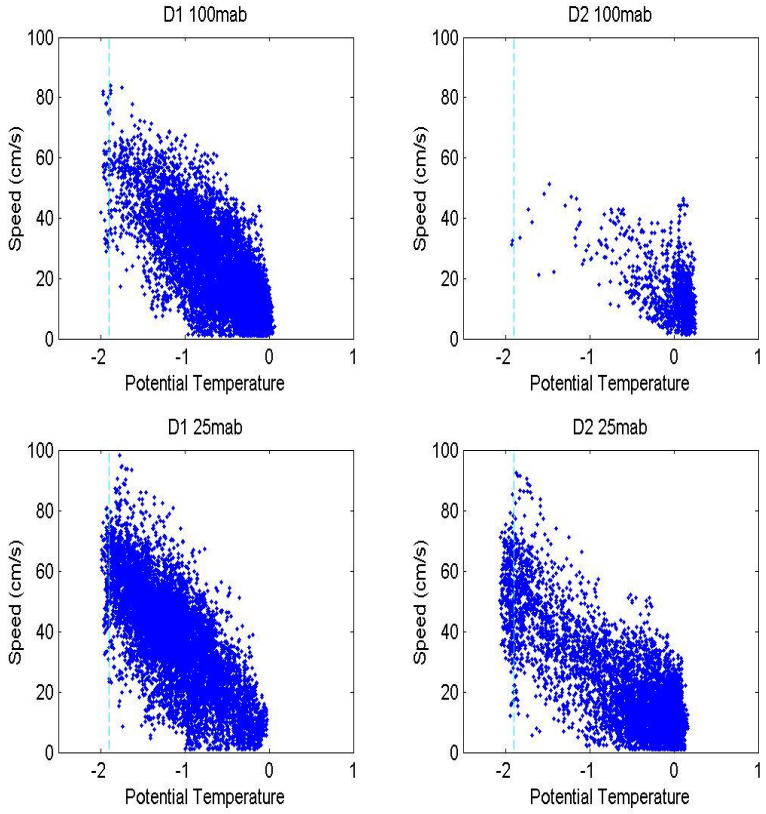

Fig.8. Scatter plot of temperature versus speed at positions D1 and D2.

How can ISW penetrate down to such great depths?

There are two main reasons why these plumes may reach the depths beyond 2000m. Firstly, the decrease in buoyancy due to mixing is counteracted by the thermobaric effect, i.e., the increase in density with increasing pressure is larger in the cold plumes than in the adjacent WDW. This effect is clearly revealed in Fig.5 where

the density profile computed with respect to surface pressure is compared with the profile calculated with 2000db as reference pressure. It is clear from Fig.6.c that high down-slope speeds are associated with low temperatures. This means that the thermobaric effect is coming into play very efficiently enhancing the downward motion.

Secondly, from CTD observations we may estimate the phase speed for waves at the ISW- WDW inter-phase. Using the values obtained from the profiles in Fig.5, i.e. $g' = 1.4*10^{-3}$ ms^{-2} and a plume thickness D=100m, we obtain an internal phase speed of $c = (g'D)^{½} \sim 0.4$ ms^{-1}. Thus, dependent on the actual plume thickness, Fig 8 indicates that the flow at D1 and D2 often is supercritical. For supercritical flows mixing due to the formation of resonance waves and subsequent wave overturning does not take place. These dense plumes may therefore reach large depths with surprisingly little mixing. The strong correlation between high speed and low temperature at D1 and D2 (Fig. 8) supports our view of the efficiency of this mechanism.

References

Alendal, G. H. Drange and P.M. Haugan, Modelling of Deep- SEa gravity currents using an integratd plume model. In *The Polar Oceans and their Role in Shaping the Global Environment*, Geophysical Monograph 84, edited by O. M. Johannessen, R. D. Muench and J. E. Overland, pp. 237-246, AGU, Washington DC, 1994.

Foldvik, A., T. Gammelsrød and T. Tørresen, Circulation and water masses on the southern Weddell Sea shelf, in *Oceanology of the Antarctic Continental Shelf, Antarct. Res. Ser. vol. 43,* edited by S. S. Jacobs, pp. 5-20, AGU, Washington D.C., 1985.

Foldvik, A. and T. Gammelsrød, Notes on Southern Ocean hydrography, sea-ice and bottom water formation, *Palaeogeogr., Palaeoclimatol., Palaeoecol., 67,* 3-17, 1988.

Foldvik, A., T. Gammelsrød, E. Nygaard and S. Østerhus. Current measurements near Ronne Ice Shelf: Implications for circulation and melting. *J. geoph. Res.*, 106 (C3), 4463-4477, 2001.

Nicholls, K.W., S. Østerhus, K. Makinsin and M.R. Johnson, Oceanographic conditions south of Berkner Island, beneath Filchner-Ronne Ice Shelf, Antarctica. , *J. Geophys. Res., 106 ,*11481-11492, 2001

Orsi, A.H. G.C. Johnson and J.L. Bullister, Circulation, mixing and production of Antarctic bottom water. Progress in Oceanography 43, 55 – 109, 1999

Schlosser, P., Bayer, R., Foldvik, A., Gammelsrød,T., Rohardt,G. and Munnich, K.O., Oxygen 18 and Helium as tracers of Ice Shelf Water and water/ice interaction in the Weddell Sea, *J. Geophys. Res., 95 (c3),* 3253-3263, 1990.